

Compact GaSb/silicon-on-insulator 2.0x μm widely tunable external cavity lasers

RUIJUN WANG,^{1,2,4,*} ADITYA MALIK,^{1,2,4} IEVA ŠIMONYTĖ,³ AUGUSTINAS VIZBARAS,³ KRISTIJONAS VIZBARAS,³ AND GUNTHER ROELKENS^{1,2}

¹Photonics Research Group, Ghent University-imec, Technologiepark-Zwijnaarde 15 iGent, 9052 Ghent, Belgium

²Center for Nano- and Biophotonics (NB-Photonics), Ghent University, Ghent, Belgium

³Brolis Semiconductors UAB, Moletu pl. 73, LT-14259, Vilnius, Lithuania

⁴These authors contributed equally to this work

*Ruijun.Wang@intec.ugent.be

Abstract: 2.0x μm widely tunable external cavity lasers realized by combining a GaSb gain chip with a silicon photonics waveguide circuit for wavelength selection are demonstrated. Wavelength tuning over 58 nm from 2.01 to 2.07 μm is demonstrated. In the silicon photonic integrated circuit, laser feedback is realized by using a silicon Bragg grating and continuous tuning is realized by using two thermally tuned silicon microring resonators (MRRs) and a phase section. The uncooled laser has maximum output power of 7.5 mW and threshold current density of 0.8 kA/cm². The effect of the coupling gap of the MRRs on tunable laser performance is experimentally assessed. A side mode suppression ratio better than 52 dB over the full tuning range and in the optimum operation point of more than 60 dB is achieved for the laser with weakly coupled MRRs.

© 2016 Optical Society of America

OCIS codes: (140.3600) Lasers, tunable; (130.0130) Integrated optics; (250.5960) Semiconductor lasers.

References and links

1. L. S. Rothman, I. E. Gordon, Y. Babikov, A. Barbe, D. Chris Benner, P. F. Bernath, M. Birk, L. Bizzocchi, V. Boudon, L. R. Brown, A. Campargue, K. Chance, E. A. Cohen, L. H. Coudert, V. M. Devi, B. J. Drouin, A. Fayt, J.-M. Flaud, R. R. Gamache, J. J. Harrison, J.-M. Hartmann, C. Hill, J. T. Hodges, D. Jacquemart, A. Jolly, J. Lamouroux, R. J. Le Roy, G. Li, D. A. Long, O. M. Lyulin, C. J. Mackie, S. T. Massie, S. Mikhailenko, H. S. P. Müller, O. V. Naumenko, A. V. Nikitin, J. Orphal, V. Perevalov, A. Perrin, E. R. Polovtseva, C. Richard, M. A. H. Smith, E. Starikova, K. Sung, S. Tashkun, J. Tennyson, G. C. Toon, V. G. Tyuterev, and G. Wagner, "The HITRAN2012 molecular spectroscopic database," *J. Quant. Spectrosc. Radiat. Transf.* **130**, 4–50 (2013).
2. J. Hodgkinson and R. P. Tatam, "Optical gas sensing: a review," *Meas. Sci. Technol.* **24**(1), 012004 (2013).
3. Z. Li, A. M. Heidt, J. M. O. Daniel, Y. Jung, S. U. Alam, and D. J. Richardson, "Thulium-doped fiber amplifier for optical communications at 2 μm ," *Opt. Express* **21**(8), 9289–9297 (2013).
4. M. N. Petrovich, F. Poletti, J. P. Wooller, A. M. Heidt, N. K. Baddela, Z. Li, D. R. Gray, R. Slavik, F. Parmigiani, N. V. Wheeler, J. R. Hayes, E. Numkam, L. Gruner-Nielsen, B. Pálsdóttir, R. Phelan, B. Kelly, J. O'Carroll, M. Becker, N. MacSuihbne, J. Zhao, F. C. Gunning, A. D. Ellis, P. Petropoulos, S. U. Alam, and D. J. Richardson, "Demonstration of amplified data transmission at 2 μm in a low-loss wide bandwidth hollow core photonic bandgap fiber," *Opt. Express* **21**(23), 28559–28569 (2013).
5. N. Ye, M. R. Gleeson, M. U. Sadiq, B. Roycroft, C. Robert, H. Yang, H. Zhang, P. E. Morrissey, N. Mac Suihbne, K. Thomas, A. Gocalinska, E. Pelucchi, R. Phelan, B. Kelly, J. O'Carroll, F. H. Peters, F. C. Garcia Gunning, and B. Corbett, "InP-based active and passive components for communication systems at 2 μm ," *J. Lightwave Technol.* **33**(5), 971–975 (2015).
6. S. Forouhar, R. M. Briggs, C. Frez, K. J. Franz, and A. Ksendzov, "High-power laterally coupled distributed-feedback GaSb-based diode lasers at 2 μm wavelength," *Appl. Phys. Lett.* **100**(3), 031107 (2012).
7. B. Rösener, S. Kaspar, M. Rattunde, T. Töpfer, C. Manz, K. Köhler, O. Ambacher, and J. Wagner, "2 μm semiconductor disk laser with a heterodyne linewidth below 10 kHz," *Opt. Lett.* **36**(18), 3587–3589 (2011).
8. K. Vizbaras, E. Dvinelis, I. Šimonytė, A. Trinkūnas, M. Greibus, R. Songaila, T. Žukauskas, M. Kaušylas, and A. Vizbaras, "High power continuous-wave GaSb-based superluminescent diodes as gain chips for widely tunable laser spectroscopy in the 1.95–2.45 μm wavelength range," *Appl. Phys. Lett.* **107**(1), 011103 (2015).
9. B. Mroziwicz, "External cavity wavelength tunable semiconductor lasers – a review," *Opto-Electron. Rev.* **16**(4), 347–366 (2008).
10. M. Takahashi, T. Takeuchi, Y. Deki, S. Takaesu, M. Horie, T. Miyazaki, M. Kurihara, S. Watanabe, K. Suzuki, N. Sakuma, A. Kawauchi, and H. Yamazaki, "Tunable lasers based on silica waveguide ring resonators," in

- Optical Fiber Communication Conference and Exposition and The National Fiber Optic Engineers Conference, OSA Technical Digest Series (CD)* (Optical Society of America, 2007), paper OWJ1.
11. T. Takeuchi, M. Takahashi, K. Suzuki, S. Watanabe, and H. Yamazaki, "Wavelength tunable laser with silica-waveguide ring resonators," *IEICE Trans. Electron.* **E92-C(2)**, 198–204 (2009).
 12. Y.-O. Noh, H.-J. Lee, J. J. Ju, M. S. Kim, S. H. Oh, and M. C. Oh, "Continuously tunable compact lasers based on thermo-optic polymer waveguides with Bragg gratings," *Opt. Express* **16(22)**, 18194–18201 (2008).
 13. K.-J. Kim, J.-W. Kim, M.-C. Oh, Y.-O. Noh, and H.-J. Lee, "Flexible polymer waveguide tunable lasers," *Opt. Express* **18(8)**, 8392–8399 (2010).
 14. T. Chu, N. Fujioka, and M. Ishizaka, "Compact, lower-power-consumption wavelength tunable laser fabricated with silicon photonic-wire waveguide micro-ring resonators," *Opt. Express* **17(16)**, 14063–14068 (2009).
 15. T. Kita, R. Tang, and H. Yamada, "Narrow spectral linewidth silicon photonic wavelength tunable laser diode for digital coherent communication system," *IEEE J. Sel. Top. Quantum Electron.* **22(6)**, 1500612 (2016).
 16. J. C. Hulme, J. K. Doyle, and J. E. Bowers, "Widely tunable Vernier ring laser on hybrid silicon," *Opt. Express* **21(17)**, 19718–19722 (2013).
 17. N. Kobayashi, K. Sato, M. Namiwaka, K. Yamamoto, S. Watanabe, T. Kita, H. Yamada, and H. Yamazaki, "Silicon photonic hybrid ring-filter external cavity wavelength tunable lasers," *J. Lightwave Technol.* **33(6)**, 1241–1246 (2015).
 18. J. H. Lee, I. Shubin, J. Yao, J. Bickford, Y. Luo, S. Lin, S. S. Djordjevic, H. D. Thacker, J. E. Cunningham, K. Raj, X. Zheng, and A. V. Krishnamoorthy, "High power and widely tunable Si hybrid external-cavity laser for power efficient Si photonics WDM links," *Opt. Express* **22(7)**, 7678–7685 (2014).
 19. S. Dhoore, L. Li, A. Abbasi, G. Roelkens, and G. Morthier, "Demonstration of a discretely tunable III-V-on-silicon sampled grating DFB laser," *IEEE Photonics Technol. Lett.* **28(21)**, 2343–2346 (2016).
 20. G. Roelkens, U. Dave, A. Gassenq, N. Hattasan, B. Chen Hu, F. Kuyken, A. Leo, M. Malik, E. Muneeb, D. Ryckeboer, S. Sanchez, R. Uvin, Z. Wang, R. Hens, Y. Baets, F. Shimura, B. Gencarelli, R. Vincent, J. Loo, L. Van Campenhout, J.-B. Cerutti, E. Rodriguez, M. Tournie, Xia Chen, M. Nedeljkovic, G. Mashanovich, Li Shen, N. Healy, A. C. Peacock, Xiaoping Liu, R. Osgood, and W. M. J. Green, "Silicon-based photonic integration beyond the telecommunication wavelength range," *IEEE J. Sel. Top. Quantum Electron.* **20(4)**, 394–404 (2014).
 21. A. Spott, M. Davenport, J. Peters, J. Bovington, M. J. R. Heck, E. J. Stanton, I. Vurgaftman, J. Meyer, and J. Bowers, "Heterogeneously integrated 2.0 μm CW hybrid silicon lasers at room temperature," *Opt. Lett.* **40(7)**, 1480–1483 (2015).
 22. R. Wang, S. Sprengel, G. Boehm, M. Muneeb, R. Baets, M. C. Amann, and G. Roelkens, "2.3 μm range InP-based type-II quantum well Fabry-Perot lasers heterogeneously integrated on a silicon photonic integrated circuit," *Opt. Express* **24(18)**, 21081–21089 (2016).

1. Introduction

Tunable semiconductor lasers operating around 2 μm wavelength have attracted a lot of interest for molecular spectroscopy as CO_2 and other atmospheric trace gases have strong and dense absorption lines in this wavelength range [1]. For tunable diode laser absorption spectroscopy (TDLAS), continuous-wave (CW) operated laser diodes with wide tuning range are required for high-performance trace gas analyzers [2]. Besides, 2 μm wavelength tunable lasers are also key components for recently developed 2 μm telecommunication systems [3, 4]. For the 2 μm wavelength range, GaSb-based and InP-based materials can be used to realize high performance semiconductor lasers [5, 6]. The integration of a semiconductor gain chip with an external cavity is an attractive solution to realize tunable single mode lasers [7, 8]. External cavity lasers can provide much wider tuning and narrower linewidth compared with vertical cavity surface emitting lasers (VCSEL) and distributed feedback (DFB) lasers. However, traditional external cavity semiconductor lasers (e.g. based on the Littrow configuration) require a bulky optics system and mechanical controllers [9]. Therefore, more compact, lightweight and cost-effective 2 μm tunable semiconductor lasers are required for e.g. portable spectroscopic sensing systems.

Passive photonic integrated circuits (PICs) can be used to provide external feedback to a III-V gain chip in order to realize compact widely tunable lasers [10–15]. Among different integrated photonics platforms, silicon photonics attracts a lot of interest since it takes advantage of mature CMOS processes, allowing the fabrication of compact photonic circuits at low cost. In the last years, III-V-on-silicon widely tunable lasers fabricated with silicon photonics technology operating at 1.55 μm wavelength have been demonstrated in various ways, including the heterogeneous integration of III-V material on silicon through bonding technology and the butt coupling of a III-V gain chip to a silicon waveguide feedback circuit [16–19]. These widely tunable lasers were realized by using silicon microring resonators

(MRRs) or sampled gratings as tunable filters. Recently, silicon-based PIC technology has been extended to the 2 μm wavelength range and beyond for spectroscopic applications [20]. 2 μm InP-based type-I Fabry-Perot lasers and 2.3 μm InP-based type-II Fabry-Perot lasers heterogeneously integrated on silicon waveguides were demonstrated based on molecular bonding and adhesive bonding technology, respectively [21, 22]. However, silicon photonics based widely tunable lasers in the 2 μm wavelength range still need to be demonstrated. In this wavelength range, GaSb-based light sources have higher performance than currently available InP-based devices. But the heterogeneous integration processes of GaSb-based active devices on silicon are less mature than that of InP-based devices, which eventually results in lower device yield and performance for the former [20].

In this paper, we report compact tunable external cavity lasers by butt coupling a GaSb-based gain chip and a silicon PIC, thereby avoiding the heterogeneous integration. A silicon spot size converter (SSC) is designed to realize efficient butt coupling between the GaSb gain chip and the silicon PIC. The silicon waveguide circuit consists of a silicon distributed grating reflector (DBR), two thermally tunable silicon MRRs and a thermal phase shifter. A tuning range of 58 nm is demonstrated. We experimentally present the effect of the coupling coefficient of the MRRs on the performance of the external cavity lasers. The uncooled lasers have a threshold current density of 0.8 kA/cm^2 and maximum output power of 7.5 mW. The measured side mode suppression ratio (SMSR) is higher than 52 dB over the full tuning range and in the optimum operation point more than 60 dB for the devices with weakly coupled MRRs.

2. Design and fabrication

The lasers consist of a GaSb-based gain chip and a silicon photonics external cavity, as schematically shown in Fig. 1.

The GaSb-based gain structure is epitaxially grown on a 3-inch Te-doped GaSb substrate by a molecular beam epitaxy system. Compressively strained $\text{Ga}_{0.7}\text{In}_{0.3}\text{As}_{0.03}\text{Sb}_{0.97}$ quantum-wells separated by $\text{Al}_{0.1}\text{Ga}_{0.9}\text{As}_{0.01}\text{Sb}_{0.99}$ barriers are used as the active region for the gain chip operating around 2.05 μm wavelength. After the epitaxial growth, the wafers are processed into single-angled-waveguide gain chips. For single-spatial mode operation, a ridge of 5 μm width and 2 μm height is chosen and defined using inductively-coupled plasma (ICP) etching and reactive-ion etching (RIE). The processed III-V wafer is cleaved into 2 mm long bars and AR/HR coatings are applied. A single layer of Ta_2O_5 is used as the AR coating, resulting in <0.1% reflectivity. For the HR side, a multiple quarter-wavelength stack of Si/SiO_2 is used to achieve a reflectivity above 95%. The devices are In bonded to a C-mount. The gain chips used in this work had a facet with a tilt-angle of 5.2 degrees. More details on the gain chip geometry and design considerations can be found in [8].

The silicon PICs are fabricated in a CMOS pilot line on 200 mm silicon-on-insulator (SOI) wafers with a 220 nm thick silicon device layer and a 2 μm thick buried oxide layer. Silicon waveguide structures are defined by 193 nm deep UV lithography and etched by ICP dry etching. On top of the silicon PIC, a 1.2 μm thick SiO_2 layer is deposited as the top cladding. The silicon PIC consists of 0.7 μm wide strip waveguides and 0.9 μm wide rib waveguides (70 nm shallow etched). A 10 μm long silicon waveguide tapered from 0.9 μm to 0.7 μm is used as a SSC to convert the optical mode between the strip waveguide and rib waveguide. The simulated reflection and loss in the strip/rib waveguide SSC is lower than -50dB and 0.2 dB, respectively. The measured propagation loss of the strip waveguide and rib waveguide is 1.8 dB/cm and 0.6 dB/cm for TE-polarized light at 2 μm wavelength, respectively. The MRRs and bus waveguides are based on rib waveguides which have lower propagation loss and allow realizing MRRs with higher Q-factor, while the phase section is implemented as a spiral-shaped strip waveguide to allow a small footprint. A Fabry-Perot laser cavity is formed between the HR-coated gain chip facet and a silicon waveguide DBR, resulting in a total cavity length of 5 mm. The DBR consists of two 250 nm wide slits spaced

500 nm, etched through the 220 nm silicon device layer. Simulations show that the DBRs have a reflectivity of more than 65% in the 2 μm wavelength range (TE-polarization) as shown in Fig. 1(b). A scanning electron microscope (SEM) image of the fabricated DBR is shown in Fig. 1(c). The silicon photonics external cavity contains a Vernier filter consisting of two thermally tuned MRRs and a phase section to set the laser wavelength, allowing continuous tuning. A 100 nm thick Ti/Au layer is deposited on the MRRs as heaters for thermal tuning of the laser wavelength. The silicon output waveguide is connected to a fiber-to-chip grating coupler to interface with standard single mode optical fiber. Simulations indicate that the back-reflection from the grating couplers to the silicon waveguides is below -25 dB in the 2 μm wavelength range. A microscope image of the silicon PIC is shown in Fig. 1(d).

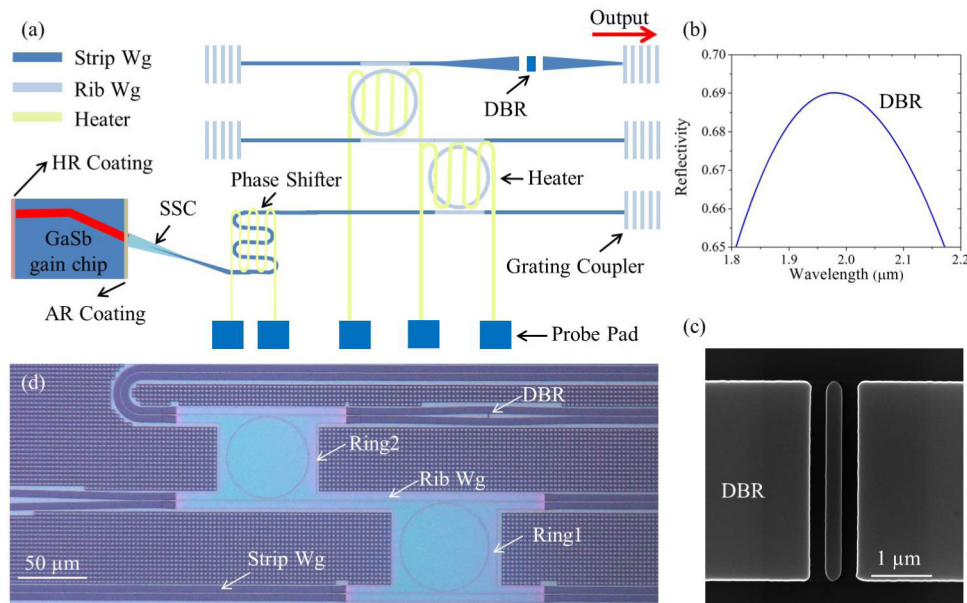


Fig. 1. (a) Schematic of a tunable GaSb-silicon external cavity laser using a silicon PIC as the feedback circuit; (b) simulated reflectivity of the DBR outcoupling mirror; (c) SEM image of the fabricated DBR; (d) microscope image of the silicon Vernier filter.

For the GaSb-based gain chip used in this work, the optical mode field diameter at the facet is $4.72 \mu\text{m} \times 1 \mu\text{m}$ (width \times height). The III-V waveguide angle at the facet is 5.2 degrees, which corresponds to an emission angle of 19.5 degrees in air. The butt coupling between the GaSb gain chip and silicon PIC is realized by a silicon SSC, schematically shown in Fig. 2(a). At the silicon SSC facet, a $6 \mu\text{m} \times 0.06 \mu\text{m}$ silicon slab waveguide tilted 12 degrees is used to achieve good coupling between the silicon SSC and III-V waveguide. A top view microscope image of the silicon SSC is shown in Fig. 2(b). Figure 2(c) shows the TE-polarized fundamental mode intensity distribution at the facet of the silicon SSC. Simulations indicate a butt-coupling loss of 1 dB at the GaSb/silicon slab waveguide interface. In order to efficiently convert the mode from the slab waveguide to that of the single mode strip waveguide ($0.7 \mu\text{m} \times 0.22 \mu\text{m}$), a 200 μm long silicon taper structure is used in the SSC. Figure 2(d) shows the simulated mode conversion loss in the slab/strip waveguide SSC as a function of the taper tip width. Considering the fabrication capabilities of the CMOS line, a 180 nm wide taper tip is used. The calculated reflection in this slab/strip waveguide SSC is lower than -30 dB. A SEM image of the silicon taper tip is shown in the inset of Fig. 2(d).

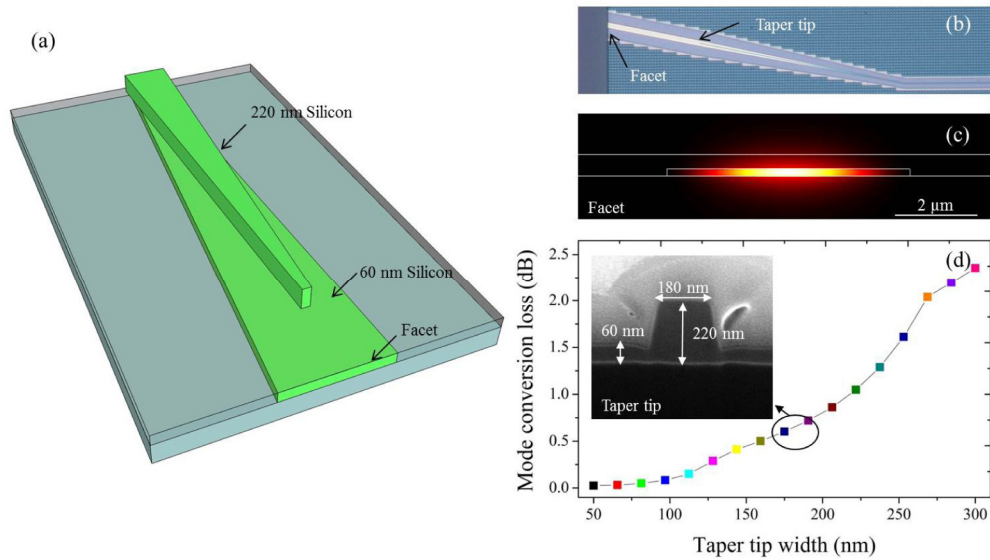


Fig. 2. (a) Schematic of the silicon SSC; (b) microscope image of the silicon SSC; (c) TE-polarized fundamental mode intensity distribution at the facet of the SSC at a wavelength of 2 μm ; (d) simulated mode conversion loss for SSCs with different taper tip width, a SEM image of the 180 nm wide taper tip is shown in the inset.

Silicon MRRs are used here as filters to select the lasing wavelength out of the Fabry-Perot cavity modes. Therefore, the free spectral range (FSR) of the filter should be larger than the bandwidth of the amplified spontaneous emission (ASE) spectrum of the gain chip to achieve stable single mode lasing. The radius of the microring should be smaller than 3.5 μm if a single resonator is used to achieve an FSR larger than 50 nm. In that case, the ring resonator quality factor would be compromised by the severe leakage loss in the ring resonator structure. In this work, a cascade of two silicon MRRs, acting as a Vernier filter, is used to achieve single mode lasing and wide tuning. Figure 3(a) shows the calculated transmission spectra of two MRRs with FSR of 6 nm and 6.5 nm at 2.03 μm wavelength, assuming a coupling coefficient $\kappa = 0.3$ and no waveguide loss. As the FSR of both the MRRs is slightly different, the individual transmission peaks are slightly shifted with respect to each other. The transmission spectrum of the Vernier filter is shown in Fig. 3(b), which is the product of transmission spectra of the two MRRs. The transmittance reaches a maximum where the resonant peaks of the individual ring resonators overlap, which determines the lasing wavelength of the external cavity laser. By thermally adjusting the position of the overlapping transmission peaks the lasing wavelength can be tuned. The tuning range is limited by the FSR of the Vernier filter, which is given by:

$$\Delta\lambda = \left| \frac{FSR1 \cdot FSR2}{FSR1 - FSR2} \right| \quad (1)$$

where FSR1 and FSR2 are the FSRs of the two MRRs. In this work, the Vernier filter consists of two MRRs with designed FSR of 6 nm (Ring1, corresponding to a ring radius of 31.5 μm) and 6.5 nm (Ring2, corresponding to a ring radius of 29 μm).

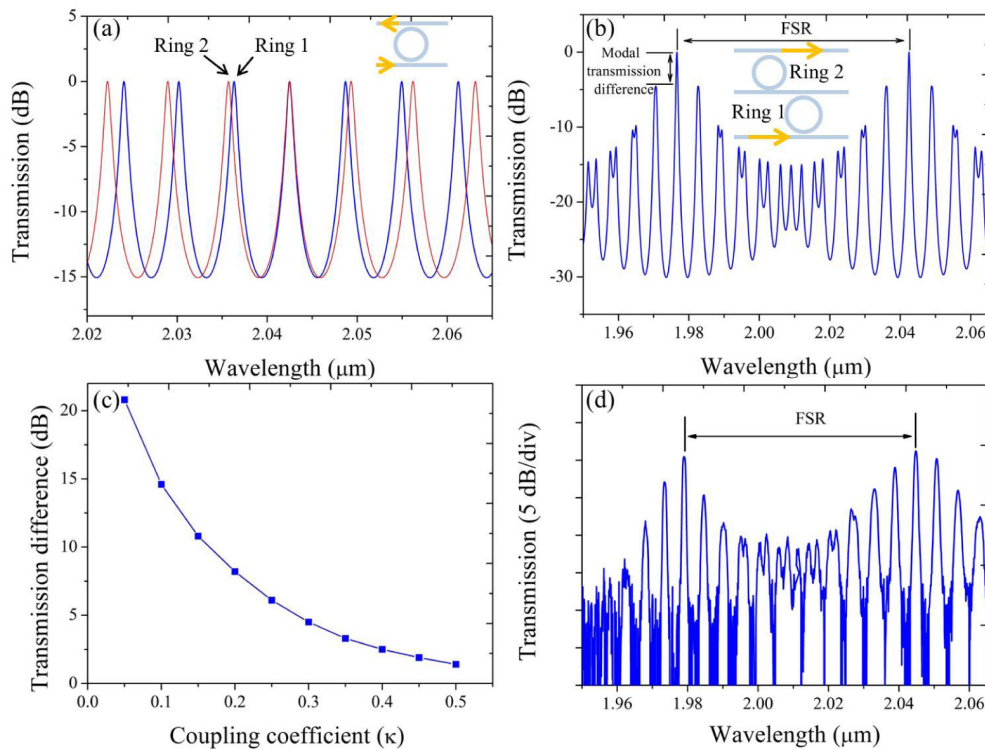


Fig. 3. (a) Simulated transmission spectra of two different MRRs with coupling coefficient $\kappa = 0.3$; (b) transmission spectrum of the Vernier filter; (c) modal transmission difference between the dominant lasing mode and the nearest side-mode as a function of the coupling coefficient of the MRRs; (d) measured transmission spectrum of the Vernier filter consisting of MRRs with coupling coefficient $\kappa = 0.3$.

The modal transmission difference between the dominant lasing mode and the nearest side-mode [marked in Fig. 3(b)] can significantly affect the SMSR and stability of the laser. The calculated dependence of the transmission difference on the coupling coefficient of the MRRs is shown in Fig. 3(c). It can be found that the transmission difference monotonically decreases as the coupling coefficient increases. The coupling coefficient can be controlled by adjusting the coupling gap between the MRRs and bus waveguides. In this work, three pairs of MRRs with coupling gap of 200nm, 350 nm and 500 nm are used in the laser feedback circuit, which have a simulated coupling coefficient κ of around 0.3, 0.13 and 0.06 at a wavelength of 2 μm , respectively. The measured quality factor of the fabricated MRRs is 2500, 6500 and 13500 around 2 μm wavelength respectively. Figure 3(d) shows the measured transmission spectrum of the Vernier filter with coupling coefficient $\kappa = 0.3$. The modal transmission difference is lower than simulated value shown in Fig. 3(b) since the transmission spectra of the two MRRs are not perfectly aligned by through thermal tuning.

3. Laser characterization

The external cavity laser characterization is carried out by mounting the GaSb-based gain chip-on-carrier and the silicon PIC on XYZ precision alignment stages. Light is coupled between the gain chip and the silicon PIC by butt coupling the two chips. The light is coupled out from the silicon waveguide through a grating coupler and collected by a standard single mode fiber (SMF-28), which is connected to an optical spectrum analyzer (OSA, Yokogawa AQ6375) measuring at a resolution of 0.05nm. The optical alignment between the two chips is performed by maximizing the light output power from the grating coupler. The laser output

power coupled to the silicon waveguide is calculated by measuring the coupling efficiency of a reference grating coupler. The coupling efficiency at $2\ \mu\text{m}$ is $-10\ \text{dB}$, and the $3\ \text{dB}$ bandwidth is $80\ \text{nm}$. During all the measurements, the GaSb gain chip operates un-cooled.

Figure 4(a) shows the light-current-voltage (L-I-V) curve of the three external cavity lasers with different coupling gaps (200 nm, 350 nm and 500 nm) between the two MRRs and bus waveguide. The waveguide referenced L-I curves are measured at a lasing wavelength of $2060\ \text{nm}$. The threshold current density and maximum output power is $0.8\ \text{kA/cm}^2$ and $7.5\ \text{mW}$ respectively for the device with a 200 nm coupling gap in the MRRs. When the coupling gap is increased to 500 nm, the threshold current density increases to $1\ \text{kA/cm}^2$ and the maximum output power reduces to $3.8\ \text{mW}$, which is attributed to the lower transmission of the ring resonator as the coupling gap increases (i.e. the ring resonator becomes undercoupled). The kinks in the L-I curve are the result of mode hopping in the laser cavity. From the three L-I curves presented here, it can be found that the laser with the weakest coupled MRRs shows the most stable operation, while the laser with smallest coupling gap shows strong mode hopping behavior. A typical emission spectrum from the laser with 500 nm coupling gap is shown in Fig. 4(b). Single mode lasing with a SMSR higher than $60\ \text{dB}$ is obtained. The corresponding electro-optic conversion efficiency is $\sim 2.3\%$ for the $7.5\ \text{mW}$ maximal output power, which is lower than the value of the external cavity laser using a bulky optics system ($\sim 3.4\%$) as shown in [8]. The laser wall-plug efficiency can be improved by further reducing the butt coupling loss at the GaSb/silicon interface, propagation loss of the silicon waveguides and the drop efficiency of the ring resonators.

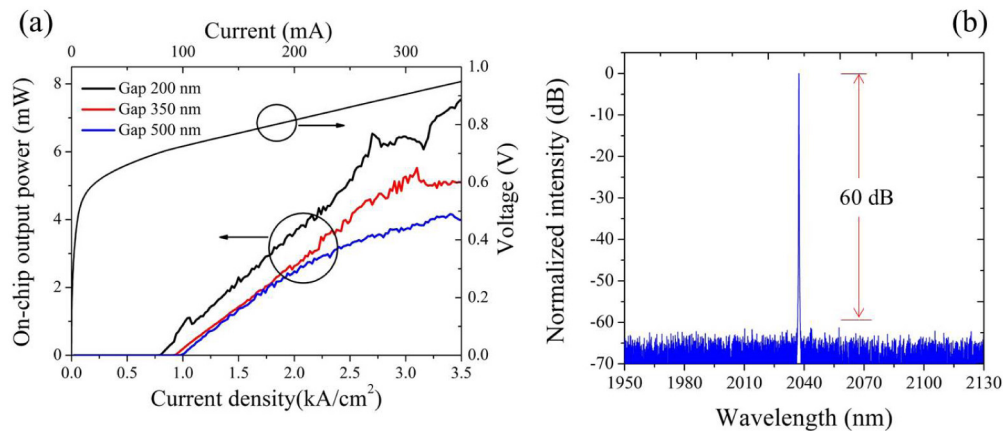


Fig. 4. (a) Light-current-voltage curves of the GaSb-silicon external cavity lasers. Three devices with different coupling gap are shown; (b) a typical output spectrum from the laser with coupling gap of 500 nm, measured at an injection current of 300 mA.

Wavelength tuning is realized by adjusting the power dissipated in the micro-heaters on top of the ring resonators and phase section. Figures 5(a)-5(c) shows the superimposed (normalized) laser emission spectra of the three tunable lasers, by tuning only one ring resonator. As discussed above, changing the temperature of one ring resonator shifts its transmission spectrum and thus the overlapping wavelength jumps from one transmission peak of the unheated ring resonator to the next. The spacing of these peaks is found to be $6.5\ \text{nm}$, which corresponds to the FSR of the unheated ring. It can be found that the SMSR of the three lasers increases as the coupling gap increases as shown in Figs. 5(a)-5(c). This is because the Vernier filter with weaker coupled MRRs has higher modal transmission difference. The current injected in the gain chip is kept at $300\ \text{mA}$ during the measurements.

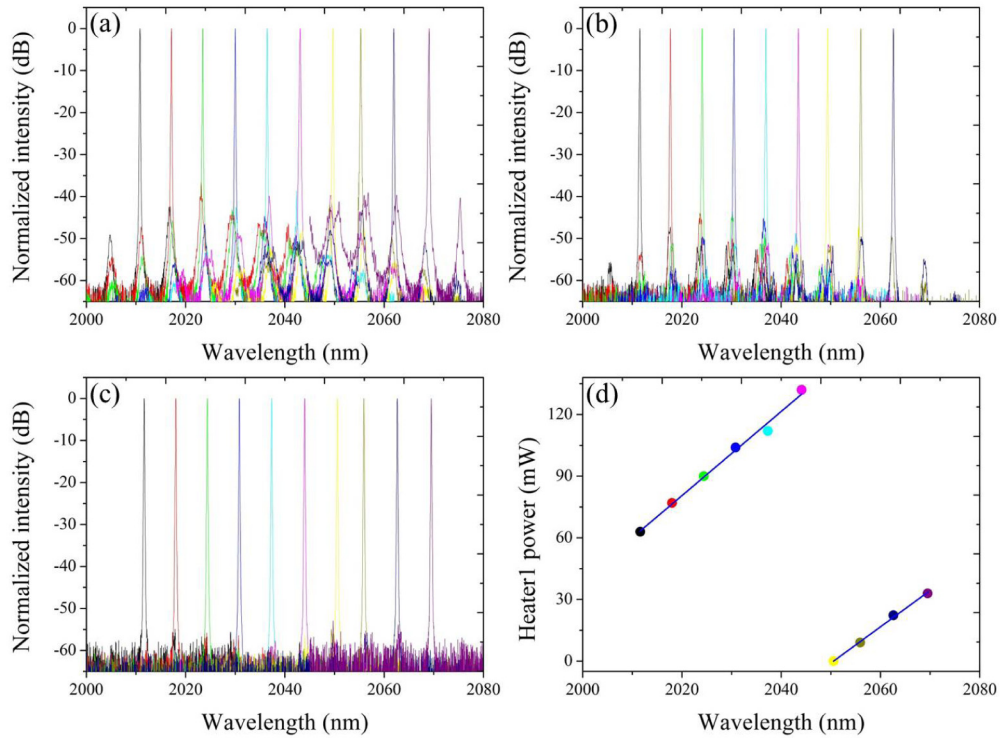


Fig. 5. Superimposed spectra of three lasers with coupling gap of 200 nm (a), 350 nm (b) and 500 nm (c), tuned by varying the heater power of Ring1; (d) wavelength tuning as a function of Heater1 power, for the case of MRRs with a coupling gap of 500 nm.

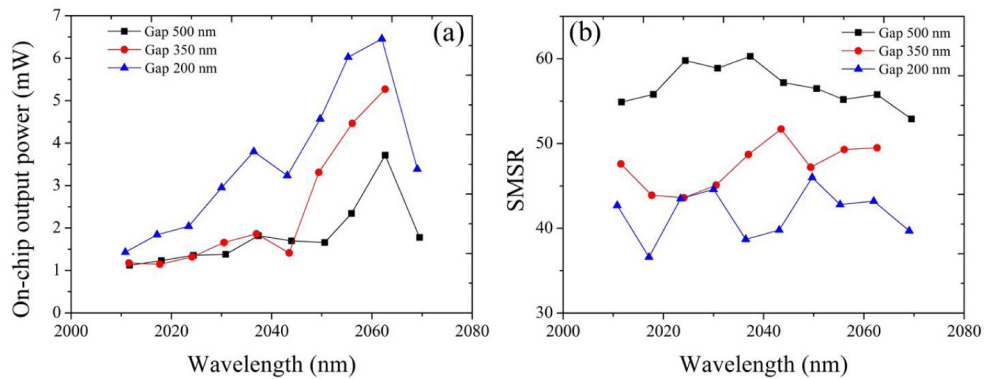


Fig. 6. Dependence of on-chip output power (a) and SMSR (b) on the lasing wavelength for the lasers with different coupling gap.

The dependence of the lasing wavelength on the power dissipated in Heater1 is shown in Fig. 5(d), for the case of MRRs with a coupling gap of 500 nm. A tuning range of 58 nm is obtained with a heater power consumption of 132 mW. This power efficiency can be improved by optimizing the heater design. In this work, heaters consisting of metal spirals covering the whole MRRs are used. More efficient heaters can be made by overlapping the metal wires with the silicon waveguide, or by providing a better thermal isolation of the ring resonators. The dependence of the output power and SMSR on the lasing wavelength for an injection current of 300 mA is shown in Figs. 6(a) and 6(b), respectively. It can be seen that the laser with smaller coupling gap has higher output power, due to the reduced internal

losses of the external cavity. The overall trend of output power on lasing wavelength matches the amplified spontaneous emission (ASE) spectrum of the gain chip [8]. The power dip at 2040 nm observed for the device with coupling gap of 200 nm and 350 nm is currently not well understood. The lasers with a coupling gap of 200 nm, 350 nm and 500 nm have a SMSR better than 36 dB, 43 dB and 52 dB over the full tuning range, respectively. The best SMSR is higher than 60 dB.

When only one of the MRRs is tuned, the wavelength resolution of tuning is limited by the FSR of the MRRs. To achieve fine tuning, both of the MRRs should be simultaneously tuned. Figures 7(a) and 7(b) show the superimposed spectra with 0.7 nm (a) and 0.2 nm (b) resolution tuning over 25 nm and 2 nm, respectively. Power efficient tuning to a specific wavelength can be realized using the following two steps. Firstly, the lasing wavelength is tuned to the position close to the targeted wavelength by heating only one MRR as shown in Fig. 6. Then, the resonant peaks of the two MRRs are moved together by increasing the dissipated power in the micro-heaters on both ring resonators. An example of this method is shown in Figs. 7(b) and 7(c), covering the 2031-2033 nm wavelength range. By dissipating 105 mW power in Heater1, the lasing wavelength is adjusted to 2031 nm as shown in Fig. 5(d). Then by increasing the power dissipated in both heaters, the lasing wavelength is tuned with a fine wavelength step.

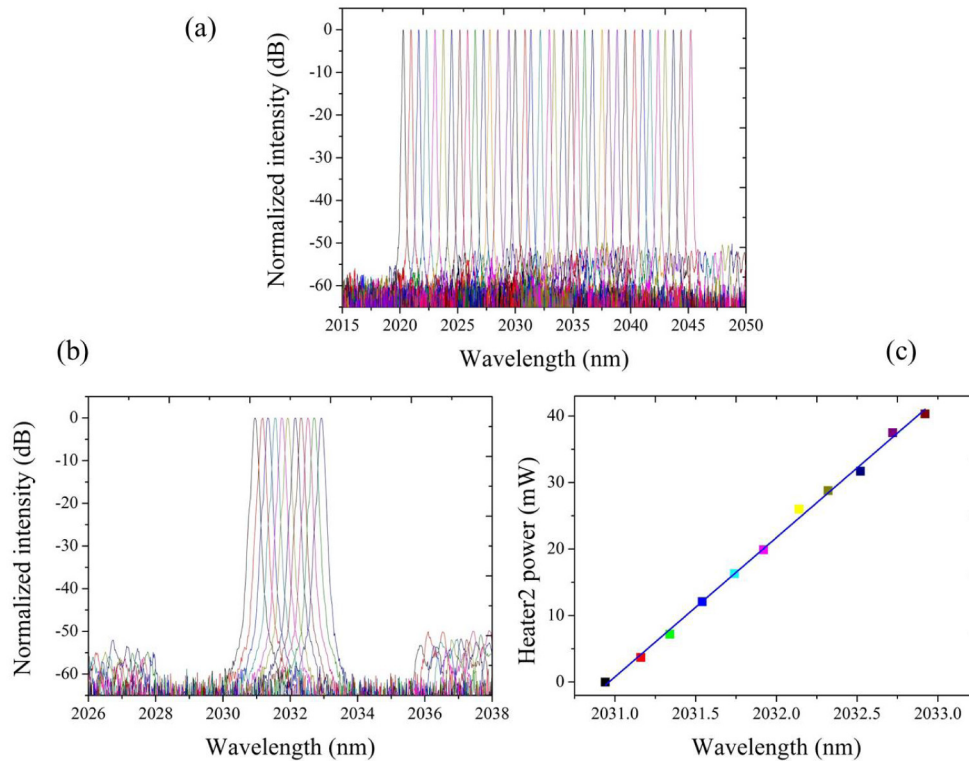


Fig. 7. Superimposed spectra of the laser with 500 nm coupling gap showing 0.7 nm (a) and 0.2 nm (b) resolution tuning over 25 nm and 2 nm, respectively; (c) dependence of the lasing wavelength on the power of Heater2 for the 0.2 nm resolution tuning shown in (b).

The wavelength resolution of tuning by two heaters is limited by the FSR of the longitudinal modes of the Fabry-Perot cavity. To achieve a continuous and more precise wavelength tuning (<0.1 nm), a heated 350 μm long silicon spiral waveguide structure is used in the laser cavity to control the position of the longitudinal modes in the laser cavity. Figure 8 shows a contour map of the fiber-coupled laser spectra as a function of the dissipated power

in the heater of the phase shifter of the device with 500 nm coupling gap. A continuous tuning with span around 0.1 nm is achieved with a power consumption of 60 mW. In this operation, the optical length of the laser cavity continuously increases as the heater power increases, which results in a red shift of the longitudinal modes. In this fine tuning, the laser with weakly coupled MRRs show more stable tuning than the devices with strongly coupled MRRs.

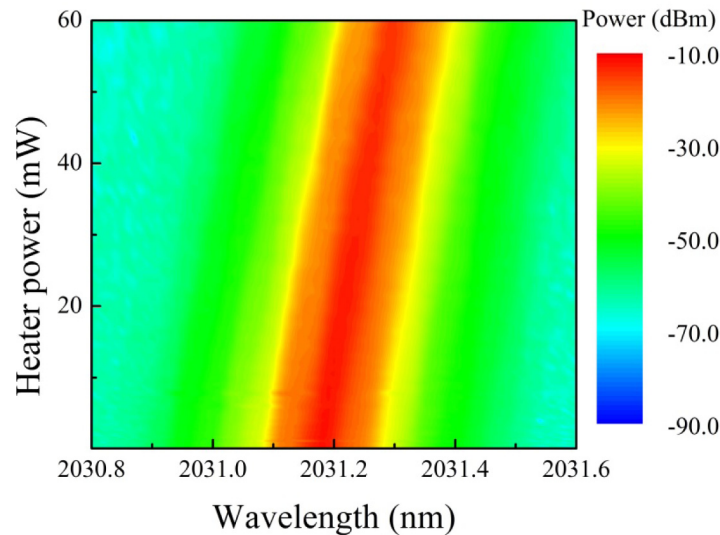


Fig. 8. Contour map of the fiber-coupled laser spectra as a function of the dissipated power in the heater of the phase shifter of the laser with 500 nm coupling gap.

4. Conclusion

In this paper, we report 2 μm wavelength range widely tunable GaSb-based external cavity lasers using a silicon photonics feedback circuit. In the feedback circuit, the lasing wavelength is selected and thermally tuned by utilizing the Vernier effect of two cascaded silicon MRRs. A phase shifter structure is used in the silicon PIC to achieve continuous tuning. A 58 nm tuning range is achieved in the 2.01-2.07 μm range. We experimentally present the effects of the coupling coefficient of the MRRs on the performance of the tunable laser. With strongly coupled MRRs, the laser has higher output power and lower threshold current, while the SMSR and tuning stability is lower than for a laser with weakly coupled MRRs. The uncooled laser has maximum output power of 7.5 mW and threshold current density of 0.8 kA/cm² when the coupling gap of the MRRs is 200 nm. A SMSR higher than 52 dB over the full tuning range and in the optimum operation point above 60 dB are obtained for the laser with weakly coupled MRRs. This result enables the implementation of compact, high performance tunable laser sources for the 2 μm wavelength range.

Funding

This work was supported by FP7-ERC-MIRACLE, FP7-ERC-PoC-FireSpec and FP7-ERC-InSpectra.

Acknowledgment

The author would like to thank S. Verstuyft and M. Muneeb for processing help and L. Van Landschoot for SEM.